Coherent-potential approximation calculations in compositionally disordered quantum wires: density of states



1992 J. Phys.: Condens. Matter 4 2565

(http://iopscience.iop.org/0953-8984/4/10/019)

J. Phys.: Condens. Matter 4 (1992) 2565–2576. Printed in the UK

# Coherent-potential approximation calculations in compositionally disordered quantum wires: density of states

K Nikolić and A MacKinnon

The Blackett Laboratory, Imperial College, Prince Consort Road, London SW7 2BZ, UK

Received 13 December 1991

**Abstract.** We have investigated the influence of different types of disorder on the electronic density of states in compositionally disordered quantum wires, using the tight-binding, coherent-potential approximation (CPA). In order to embed the correlations that are present in any wire structure the single-site CPA condition $\langle t_i' \rangle_{\text{config}} = 0$, has been generalized to the matrix equation for a slice ($L$) of the wire as a scatterer $\langle t_L' \rangle_{\text{config}} = 0$. Essentially this approximation is similar to the molecular CPA (MCPA) or the cluster CPA but due to the geometry of the system translational invariance along the effective wire is not broken. Calculations for monolayer wires reveal that the boundary roughness of a wire degrades the ideal quasi-one-dimensional density of states in a characteristic way. This degradation is even stronger in the presence of islands. The subband representation reveals that the density of states in each channel is affected by the edge disorder in proportion to the Fermi energy or channel number. By contrast the effect of the presence of islands is independent of the channel number.

## 1. Introduction

Quantum wire structures have density of states features which are very useful for laser and other applications and they have been predicted to have extremely high electron mobilities [1]. Also, in laser applications, a smaller current threshold density and better temperature stability [2] is possible than in lasers produced from higher dimensional structures. An important question is how compositional disorder affects the above mentioned attractive features of quantum wires. It has already been reported that the atomic structure of interfaces between GaAlAs/GaAs epitaxial films grown by molecular beam epitaxy controls some of the optical properties of quantum wells [3]. Disorder induced during the production of lateral confinement in quantum wires (e.g. lithography [4] or wires grown on a vicinal surface [5]) is usually stronger than in the epitaxial layer interface. Decreasing the lateral dimensions of the wires produces a wider separation of energy subbands but interface fluctuations become more important. Also in the 1D (or quasi-1D) case there is a much higher probability of multiple scattering from the same site compared to the 2D or 3D case. This could contradict the expected extremely high mobility in quantum wires (due to suppression of both impurity and optical phonon scattering [1]).

The aim of this paper is to examine the possibility of using CPA calculations to investigate the equilibrium electronic properties of compositionally disordered quantum wires. Comparing with some common disordered systems (like random alloys),

0953-8984/92/102565+12$04.50  

peculiar to quantum wires are the specific compositional correlations (e.g. transverse and longitudinal) that a wire system might have.

We suppose that the wire atoms are located at the sites of a cubic lattice. The localized s-state atomic orbital on a site $i$ is denoted $|i\rangle$, so the one-electron tight-binding Hamiltonian for this system is given by:

$$\mathbf{H} = \sum_i |i\rangle \varepsilon_i \langle i| + \sum_{\substack{i,j \\ (i \neq j)}} |i\rangle V_{ij} \langle j| \tag{1}$$

where $\varepsilon_i$ is the 'site energy' (it corresponds to the potential energy at site $i$) and $V_{ij}$ is the hopping matrix element and we shall assume that it is zero unless the $i$ and $j$ sites are the nearest neighbours, when $V_{ij} \equiv V = 1$ (i.e. $V$ will be a unit of energy). The Green function of the system is defined by:

$$\mathbf{G}(z) = (z\mathbf{I} - \mathbf{H})^{-1}. \tag{2}$$

The CPA replaces the real medium with an effective periodic medium [6]. The effective medium is determined by the condition that the Green function of the effective medium ($\mathbf{G}_e$) is equal to the configurationally averaged Green function of the real system ($\langle \mathbf{G} \rangle_{\text{config}}$). Hence:

$$\mathbf{G}_e = (z\mathbf{I} - \mathbf{H}_e)^{-1} = \langle \mathbf{G} \rangle_{\text{config}} \tag{3}$$

where $\mathbf{H}_e$ is the effective Hamiltonian given by:

$$\mathbf{H}_e = \sum_i |i\rangle \sigma \langle i| + \sum_{i,j} |i\rangle V \langle j|. \tag{4}$$

The effective medium is described by a scalar self-energy $\sigma$. The scalar self-energy is a useful concept for an uncorrelated disordered system which is homogenous on average. But it is obvious that a quantum wire (as in figure 2, below) is not such a system, so, in general, we cannot successfully use the single-site CPA. However the single-site CPA can be used for some cases, e.g. in calculations which consider only the effect of uncorrelated islands in the perfect wire. In this case the self-energy $\sigma$ from relation (4) depends on the position of the site across the wire. Therefore this self-energy is position dependent (section 3.1). In order to treat fluctuations of the width and the centre of the wire (without the correlations from slice to slice) we have used the CPA model with the generalized condition (19)—section 3.2. In both cases, the effective medium has translational symmetry along the wire, with the periodicity equal to the lattice constant $a$. For such a system we can use a method similar to that for semi-infinite leads [11] in order to obtain the expression for the Green function. The CPA approach which includes possible longitudinal correlations rather complicates the calculations, but does not give us any new effects.

Calculations are done with GaAs/AlAs systems in mind although this treatment is general and can be applied to other material systems.

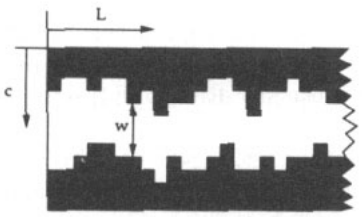


**Figure 1.** Plot of the section of quantum wire showing the meaning of the width ($w$) and the centre ($c$) of the wire.

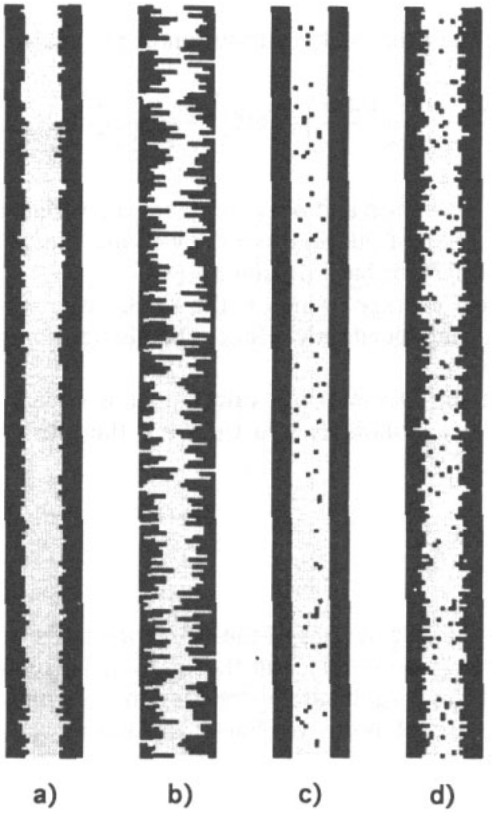


**Figure 2.** Plot of sections of the quantum wires of average width 10: (*a*) $\sigma_w^2 = 1, \sigma_c^2 = 0$, no islands; (*b*) $\sigma_w^2 = 3, \sigma_c^2 = 7.5$, no islands; (*c*) perfect wire, with addition of islands, concentration $p$=0.05; (*d*) $\sigma_w^2 = 3, \sigma_c^2 = 0$, with island concentration $p$=0.05.

## 2. Definition of the system

The monolayer quantum wire system we shall consider here is shown in figure 1 (also see figure 2 below.). The dark squares (■) correspond to an A-site and light squares to a B-site. In order to examine the edge fluctuations and the meandering of the wire, the positions of the centre ($c$) and width ($w$) are identified for each slice along the length, $L$, of the wire.

The island structures within the wires are treated independently. We assume a

Gaussian distribution for the random variables $w$ and $c$ just in order to quantify compositional disorder in these structures. We have chosen this distribution because it gives structures similar to those obtained by computer simulation of vicinal surface grown quantum wires [7]. However, we can use any distribution, since the distribution does not affect our method of calculations.

Since we have only discrete values for $w$ and $c$ we use the error function in order to define probability distributions and preserve the normalization. Hence the probability that the width of the wire is $w$ will be:

$$p(w) = \frac{1}{2}\left[\mathrm{erf}\left(\frac{w-\mu_w+0.5}{\sqrt{2\sigma_w^2}}\right) - \mathrm{erf}\left(\frac{w-\mu_w-0.5}{\sqrt{2\sigma_w^2}}\right)\right]. \tag{5a}$$

A similar expression exists for the probability distribution of the centre of the wire $c$:

$$p(c) = \frac{1}{2}\left[\mathrm{erf}\left(\frac{c-\mu_c+0.25}{\sqrt{2\sigma_c^2}}\right) - \mathrm{erf}\left(\frac{c-\mu_c-0.25}{\sqrt{2\sigma_c^2}}\right)\right]. \tag{5b}$$

Here $\mu_w$ and $\mu_c$ are the mean values and $\sigma_w^2$ and $\sigma_c^2$ are the variances of $w$ and $c$. Values of the width and the position of the centre of the wire are usually uncorrelated, e.g. for the simulation results in [7] we have obtained $|\langle(w-\mu_w)(c-\mu_c)/\sigma_w\sigma_c\rangle| \simeq 10^{-3}$ ($\langle\ \rangle$ means configurational average) which is the same order of magnitude as obtained for $w$ and $c$ generated independently. Hence the distributions (5*a*) and (5*b*) are mutually independent.

The method that we are going to use in our calculations is equally applicable to any cross section of the wire, but monolayer structures are the most convenient for efficient calculations.

## 3. Method

We first set up the method for the calculations of the effect of islands only, neglecting the boundary roughness of wires (section 3.1), and then vice versa (section 3.2). Both algorithms use the one-dimensional subband representation, but differ in the self-energy calculations. For the case of both roughness and islands we have merged these two methods (section 4).

### *3.1. Position dependent self-energy*

If the wire system can be described by defining the different concentrations of A-atoms across the wire (the host consists of B-atoms, see figure 2(*c*)), then the method uses the single-site CPA condition:

$$\langle t_i' \rangle_{\mathrm{config}} = 0 \tag{6}$$

where:

$$t_i' = \frac{\varepsilon_i' - \sigma}{1 - (\varepsilon_i' - \sigma)\mathbf{G}_e(i,i)} \tag{7}$$

and $\varepsilon_i' = \varepsilon_i - \varepsilon_B$. For $\varepsilon_A \to \infty$ and $\varepsilon_B = 0$ condition (6) gives the self-energy at the position $m$ across the wire:

$$\sigma(m) = -\frac{p_A(m)}{\mathbf{G}_e(m,m)} \qquad m = 1,2,...,M \tag{8}$$

$p_A(m)$ is the concentration of A-atoms along line $m$ in the wire and $M$ is the number of sites in a cross section of the wire. Here we have a position dependent scalar self-energy $\sigma(m)$, which could be represented as a diagonal matrix in the slice representation from section 3.2.

The expression for $\mathbf{G}_e(m,m)$ can be obtained in the following way. The $\mathbf{G}_e(m,m)$'s are the elements on the main diagonal of matrix $\mathbf{G}_d$, which corresponds to a slice of the effective wire, and by definition is the submatrix on the main diagonal of $\mathbf{G}_e$. For an infinite strip one has [11]:

$$\mathbf{G}_d \equiv \mathbf{G}_d^{(\infty)} = \left[E\mathbf{I} - \mathbf{H}_e^{(1)} - 2\mathcal{V}^\dagger \mathbf{G}_d^{(\infty/2)} \mathcal{V}\right]^{-1} \tag{9}$$

where $\mathbf{G}_d^{(\infty/2)}$ corresponds to a semi-infinite strip and is given by [11]:

$$\mathbf{G}_d^{(\infty/2)} = \left[E\mathbf{I} - \mathbf{H}_e^{(1)} - \mathcal{V}^\dagger \mathbf{G}_d^{(\infty/2)} \mathcal{V}\right]^{-1}. \tag{10}$$

$\mathbf{H}_e^{(1)}$ is the Hamiltonian for an isolated effective slice, given by equations (4) and (8), and $\mathcal{V}$ contains the nearest-neighbour hopping elements between two slices (relation (16)). Here superscripts designate the length of the system. For $\mathcal{V} = \mathbf{I}$ and in the basis of the eigenvectors of $\mathbf{H}_e^{(1)}$, relations (9) and (10) reduce to a set of scalar equations. Therefore we have for the diagonal elements of the Green function in the subband representation:

$$g_m^{(\infty)} = \pm \frac{1}{\sqrt{(E - e_m)^2 - 4}} \qquad m = 1,2,...,M \tag{11}$$

where $g_m^{(\infty)}$ are the elements of the diagonal matrix $\mathbf{U}^{-1}\mathbf{G}_d^{(\infty)}\mathbf{U}$ ($\mathbf{U}$ is the matrix of eigenvectors $\boldsymbol{u}_m$ of $\mathbf{H}_e^{(1)}$) and $e_m$ are the eigenvalues of $\mathbf{H}_e^{(1)}$. The sign of the square-root is chosen so that $\mathrm{Im}(g_m^{(\infty)})$ and the density of states have the proper sign [10,12]. Finally for $\mathbf{G}_e(m,m)$ we have:

$$\mathbf{G}_e(m,m) = \mathbf{G}_d(m,m) = \sum_{i=1}^{M} |u_i(m)|^2 g_i^{(\infty)}. \tag{12}$$

The total density of states $\rho(E)$ is defined as usual, which in our case gives:

$$\rho(E) = \frac{-1}{\pi M} \mathrm{Im}\left[\mathrm{Tr}\mathbf{G}_d(E + \mathrm{i}0)\right]. \tag{13}$$

Since we calculate $\mathbf{G}_d(m,m)$ we also have the local density of states at each site. A similar expression to (13) is that for the channel density of states, but with $g_m^{(\infty)}$ given by (11) instead of $\mathbf{G}_d$.

We shall use this approach in the case of the islands of A-atoms in the perfect wire of B-atoms. For the higher concentration of island atoms there is a higher possibility of forming clusters of island atoms, and our approximation can miss structure associated with these clusters [8(b),10]. So this approach is generally good if we have a small concentration of islands in the wire. Nevertheless conditions in our calculations (strong scattering regime, i.e. $(\varepsilon_A - \varepsilon_B)/(2V) \gg 1$) will push this part with complicated structure towards the higher energies, far from the Fermi energy.

This model fails to give good results for wires with rough boundaries because it cannot define the rough edge of the wire. Therefore, in this case we have used a further extension of the CPA, which is detailed in the next section.

### *3.2. Self-energy matrix*

If one takes into account the lateral correlations in a slice of a wire and uses the framework of CPA then it is natural to treat a whole slice as a scatterer. A wire can be divided into slices (along the wire) such that each slice may be labelled by a single integer $(L)$. A useful basis set now is the set of vectors $|L\rangle$, where $|L\rangle$ is a vector consisting of $M$ orbitals $|i\rangle$ on the $L$th slice. The Hamiltonian of our system (1) can be rewritten:

$$\mathbf{H} = \sum_L |L\rangle \mathcal{E}_L \langle L| + \sum_{\substack{L,R \\ (L \neq R)}} |L\rangle \mathcal{V}_{LR} \langle R| \tag{14}$$

where $\mathcal{E}_L$ contains matrix elements of the Hamiltonian for an isolated slice (like (1), where $|i\rangle \in |L\rangle$) and $\mathcal{V}_{LR}$ is a matrix of hopping elements between $L$th and $R$th slice. In the nearest-neighbour model $\mathcal{V}_{LR}$ is non-zero only if $R = L \pm 1$, and $\mathcal{V}_{L,L\pm1} \equiv \mathcal{V}$ is diagonal (later we shall use $\mathcal{V} = \mathbf{I}$).

Now we can replace our real wire with the periodic effective wire, formed of the same (effective) slices. The Hamiltonian of the effective wire is

$$\mathbf{H}_e = \mathbf{H}_0 + \sum_L |L\rangle \Sigma \langle L| \tag{15}$$

where $\mathbf{H}_0$ is the Hamiltonian of a uniform system (taken for example to be a lattice of B-atoms alone) given by:

$$\mathbf{H}_0 = \sum_L |L\rangle \mathcal{E}_0 \langle L| + \sum_L |L\rangle \mathcal{V} \langle L \pm 1| \tag{16}$$

and $\Sigma$ is a matrix self-energy of dimension $M \times M$. The self-energy is a symmetric, complex matrix. The perturbation Hamiltonian in this case is:

$$\mathbf{H}_1 = \mathbf{H} - \mathbf{H}_e = \sum_L |L\rangle (\mathcal{E}'_L - \Sigma) \langle L| \tag{17}$$

and

$$\mathcal{E}'_L = \mathcal{E}_L - \mathcal{E}_0. \tag{18}$$

Now we use, instead of the single-site CPA condition (6), the generalized condition [8,9]:

$$\langle t'_L \rangle_{\text{config}} = 0 \tag{19}$$

where:

$$t'_L = (\mathcal{E}'_L - \Sigma)\left[\mathbf{I} - \mathbf{G}_{e_{LL}}(\mathcal{E}'_L - \Sigma)\right]^{-1} \tag{20}$$

$t'_L$ is a $t$-matrix for a scatterer at position $L$ in the effective medium. Here $\mathbf{G}_{e_{LL}}$ is a submatrix of dimension $M \times M$ of matrix $\mathbf{G}_e$ (at the position $L, L$).

Condition (19) means that a slice embedded in the effective medium, on average, produces no scattering. This matrix generalization of the single-site CPA retains the analytic properties of the CPA, in the same way as the MCPA (which is proved by Ducastelle in [9]). Here we do not have problems with the broken translational invariance because the effective wire, formed of the effective slices, keeps the translational symmetry of the lattice along the wire. At the lateral boundaries of the system the wave function is forced to have nodes. Therefore the self-energy operator is still block-diagonal (or cluster-diagonal, as in the MCPA), but here each block has a natural meaning—it corresponds to an effective slice of the wire.

For an infinitely long effective wire, $\mathbf{G}_{e_{LL}}$ does not depend on $L$, so we shall drop subscripts $LL$ in the following text and use $\mathbf{G}_{e_{LL}} \equiv \mathbf{G}_d$. We deal with the infinitely long wire system which is equivalent to a configurational average, therefore our results will represent most probable values for the calculated features. From equations (19) and (20), after some rearrangement, we obtain a self-consistent relation for the self-energy:

$$\Sigma = \langle \mathcal{E}'_L\left[\mathbf{I} - \mathbf{G}_d(\mathcal{E}'_L - \Sigma)\right]^{-1}\rangle_{\text{config}} \tag{21a}$$

or in the form more appropriate for the long strip geometry:

$$\Sigma = \sum_{c=1}^{n_c} p_c \mathcal{E}'_c\left[\mathbf{I} - \mathbf{G}_d(\mathcal{E}'_c - \Sigma)\right]^{-1} \tag{21b}$$

where $n_c$ is the number of possible configurations of a slice, and $p_c$ is the probability that slice $\mathcal{E}'_c$ appears in the wire.

The expression for $\mathbf{G}_d$ has been obtained in section 3.1. Here the Hamiltonian for an isolated effective slice is given by:

$$\mathbf{H}_e^{(1)} = \mathcal{E}_0 + \Sigma. \tag{22}$$

Equations (11), (21) (or (8) for islands) and (22) form a self-consistent set of equations. In order to calculate the density of states this system of equations is iterated until the self-consistency is achieved. Results of numerical calculations are presented in section 4.

## 4. Results

Here we simulate GaAs/AlAs wires, so that we have $\varepsilon_{Al} \gg \varepsilon_{Ga}$, which means in our case that host B-atoms are Ga-atoms and A-atoms are Al-atoms. For $(\varepsilon_{Al} - \varepsilon_{Ga})/(2V) > 6$ the spectrum of (1) splits into two subbands centred about $\varepsilon_{Ga}$ and $\varepsilon_{Al}$ respectively [13]. The states close to the band edge of the Ga-subband are studied in our case (so the normalization factor in relation (13) can be $\langle w \rangle$ instead of $M$).

Because of the high value of the Al site energy, off-diagonal disorder is not relevant. We have adopted $\varepsilon_{Ga} = 0$, while for $\varepsilon_{Al}$ any value greater than 50 gives virtually the same result. We are not dealing with totally realistic GaAs/AlAs system, but the intention is to treat a system for which the scattering structure is similar to that of a realistic system.

We consider a system of 20 lattice sites width. Assuming that the total amount of Ga and Al atoms in the considered system are equal, each wire will be on average of width $w = 10$. Island contributions are represented simply by the random occurrence of a single Al-site instead of Ga-site. In the simulations of wires in reference [7], for example, results for a wire of width 10 show that most islands are in fact single sites. The number of larger islands are satisfactorily reproduced by the probability of several neighbouring Al-atoms.

Here we present results of the numerical calculations for several different types and degrees of disorder in quantum wires. A plot showing sections of the considered wire systems is given in figure 2.

As well as the CPA results, figures 3(*a*),(*b*),(*c*) and (*d*) also give the exact density of states as a histogram which was obtained using a method [14] based on the work by Dean and Martin [16], and revived by Evangelou [17]. Fluctuations around the true value are inevitable in these calculations of 'exact' density of states due to the finite length of system.

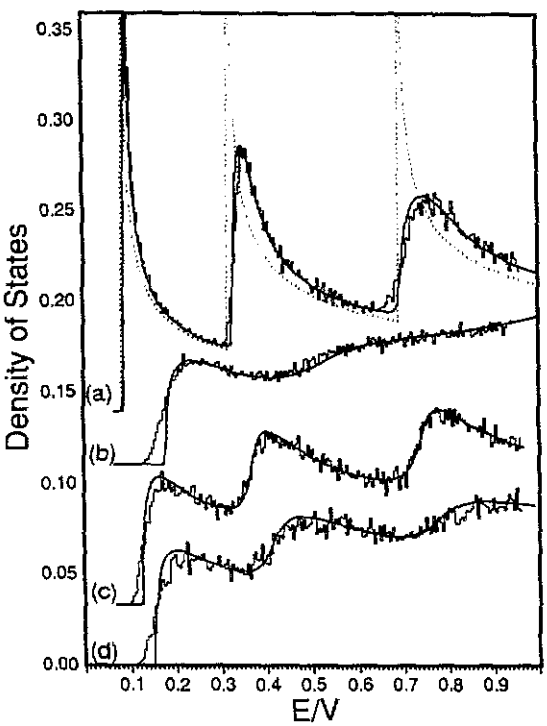


**Figure 3.** The density of states calculated using CPA and a histogram of exact DOS (calculated for $N$ slices) together with the perfect case (dotted line) corresponding to figures 2(*a*) $N=30000$, (*b*) $N=400000$, (*c*) $N=100000$, (*d*) $N=100000$. The bottom of band is shifted to 0. Curves (*a*), (*b*) and (*c*) have been shifted vertically.

Results from figure 3(*a*) indicate that the increase of width fluctuations (i.e. roughness of the boundaries of the wire) shifts the peaks towards higher energies, broadens them and decreases their magnitude. No shift of the peaks is observed when there are longitudinal correlations in the widths of the slices [14]. For a very high level of disorder (see figure 3(*b*)) the quasi one-dimensional characteristics are flattened, tending to the spectrum of 2D systems. The effects of roughness of the boundaries of the wire on the one-dimensional (1D) subband density of states are shown in the figures 4(*a*) and (*b*). The peak of the density of states in each subband broadens and decreases with increase of electron energy, i.e. the subband number. A simple physical explanation for this starts from the density of states per atom in the perfect 1D subband. For the tight-binding model and monolayer wire, this is given by:

$$\rho_0(E) = \frac{1}{\pi V\sqrt{1-((E-E_n)/2V)^2}}[\theta(E-E_n+2V)-\theta(E-E_n-2V)] \quad (23)$$

where $E_n$ is the subband edge for the $n$th ($n = 1, \ldots, M$) subband :

$$E_n = 2V\cos(n\pi a/w) \quad (24)$$

and $a$ is the lattice constant. The change in subband density of states caused by small width fluctuations ($\delta w$) can be roughly estimated from:

$$\delta\rho_0 \sim -\ n\,\frac{a}{w^2}\,\sin\left(n\pi\frac{a}{w}\right)\,\xi\,\rho_0^3(\xi)\ \ \delta w \quad (25)$$

where $\xi = (E - E_n)/2V$ is the same in each subband. Hence the edge roughness has an influence on the density of states proportional to the subband number $n$ and also to $\rho_0^3$ (therefore peaks are more affected than flat parts). The width of the wire $w$ in relation (25) is actually the effective width 'seen' by an electron on the length equal to the longitudinal wavelength of the electron $\lambda$. This means that even if the width of each slice is equal, if the position of the centre fluctuates (i.e. wire is meandering) there are still effective width fluctuations. The effect on the density of states is smaller, but still similar to width fluctuations.

The presence of the islands in the wire structures, figures 3(*c*) and (*d*), substantially degrades the peaks for even small concentrations of islands. The effect is similar in each subband (figure 4(*c*)). Since relation (8) for the self-energy in this case is not dependent on the subband index, this leads to an energy-independent broadening. The peak in the first subband is slightly higher and sharper than in the other bands, because it has limited space for broadening towards smaller energies, since the CPA does not see the tail at the beginning of density of states line.

Each 1D subband spans the whole accessible energy range, i.e. each starts from the band edge (figures 5(*a*),(*b*),(*c*)) for both types of disorder. This is due to the disorder induced hybridization effect [15] between the corresponding 1D subbands of the perfect wire. For small edge disorder one can clearly observe that the tails of the density of states lines roughly follow the perfect 1D subbands, but with very reduced magnitude (figure 5(*a*)). As disorder increases the tails rise and flatten (figure 5(*b*)).

In the calculations the relations (11), (21) (or (8)) and (22) are solved self-consistently until a relative difference of the density of states in two iterations became less then $\epsilon$ (results are virtually the same for any positive $\epsilon < 10^{-3}$). Except for a

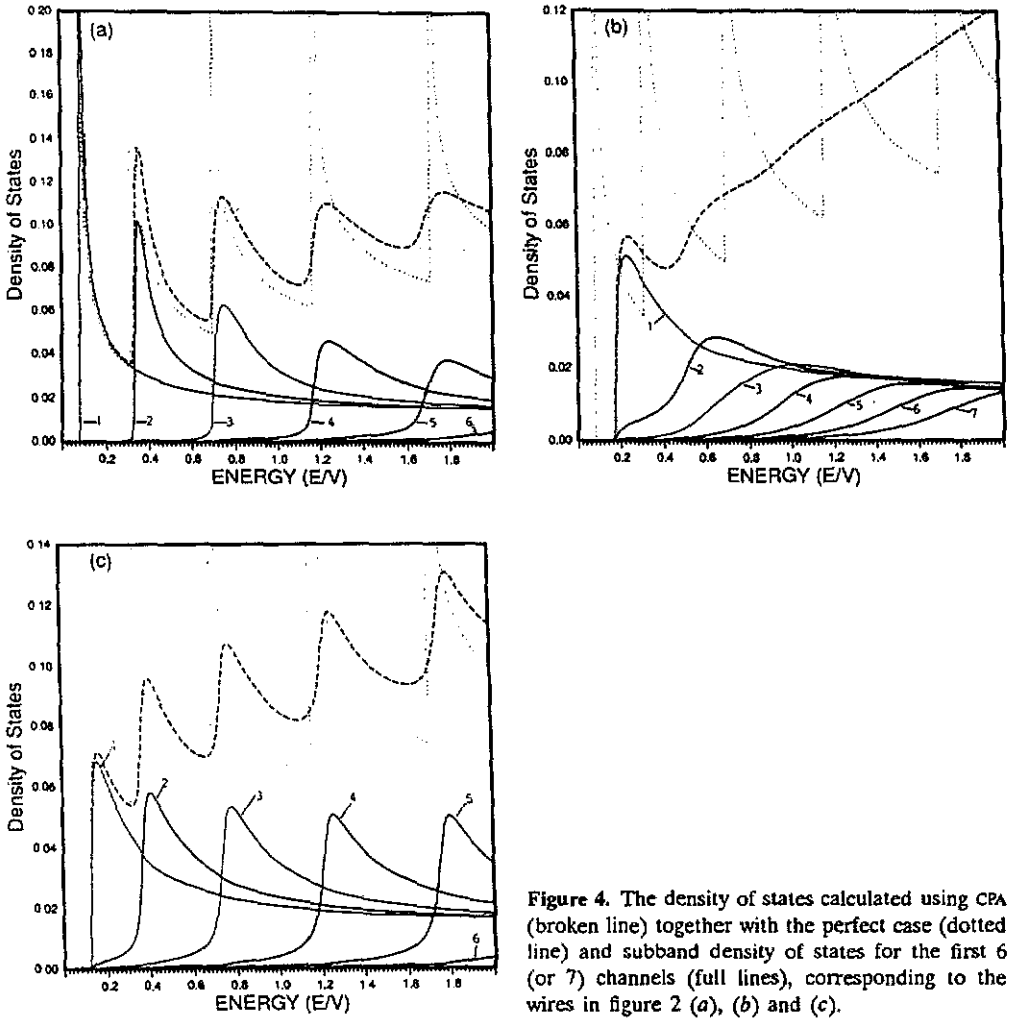


**Figure 4.** The density of states calculated using CPA (broken line) together with the perfect case (dotted line) and subband density of states for the first 6 (or 7) channels (full lines), corresponding to the wires in figure 2 (*a*), (*b*) and (*c*).

very few values of the energy, we have very rapid convergence (2–5 iterations) when the final value of self-energy $\Sigma$ for a given energy is taken as the initial matrix $\Sigma$ for the next energy. Critical values of energy occur when a new subband is reached, and then about 20–25 iterations are needed in order to obtain the desired precision.

In the case of a wire with both edge fluctuations and islands we have used combined methods from sections 3.1 and 3.2. Calculations are based on the self-consistent method as in section 3.2, but in each iteration when we obtain a new value for the matrix $\Sigma$ (from equation (21)), we rederive diagonal elements $\Sigma(m,m)$ using method 3.1, and then continue with method 3.2. New values for $\sigma(m)$ in method 3.1 are obtained using condition (6) and relation (7).

In the first iteration:

$$\sigma^{(1)}(m) = \Sigma(m,m) - \frac{p(m)}{\mathbf{G}_d(m,m)}.$$

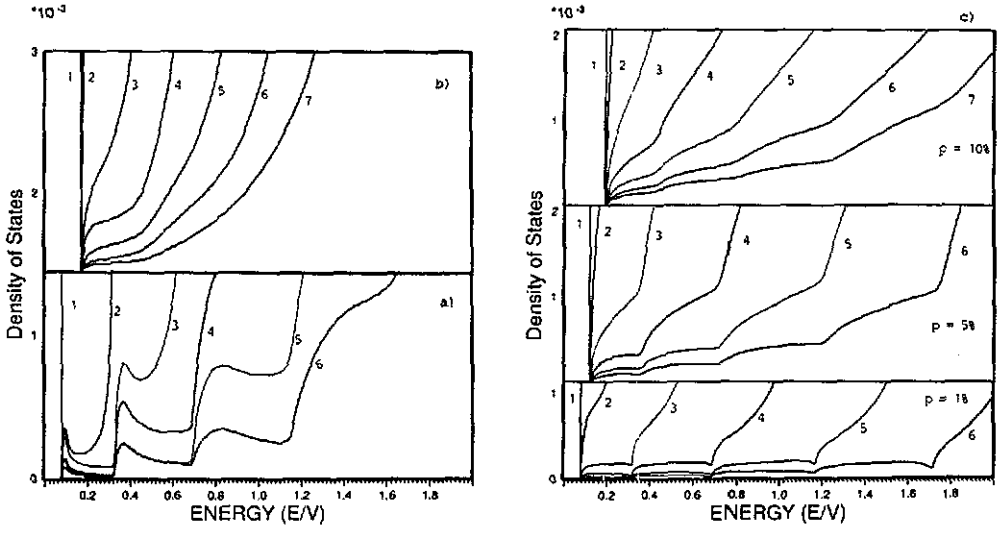


**Figure 5.** As in figure 4, but focused in the region of small density of states. Figure (*c*) contains results for island concentrations: $p = 0.01$, $p = 0.05$ and $p = 0.1$.

The $(i+1)$th iteration:

$$\sigma^{(i+1)}(m) = \sigma^{(i)}(m) - \frac{p(m)}{\mathbf{G}_{\mathrm{d}}(m,m)}$$

where $p(m)$ is the concentration of islands at position $m$ across the wire. When $\sigma(m)$ is determined with sufficient precision we go back to the matrix $\Sigma$, replacing $\Sigma(m,m) = \sigma(m)$. Here we use an effective medium, defined by matrix $\Sigma$, as a host medium, then add islands and derive a new effective medium correcting the self-energy of the sites where islands can be.

CPA gives good results in comparison with the exact density of states. Exceptions are the tails at each subband which CPA cannot provide. This is the standard failing of CPA calculations [6, 10] since this approximation takes exactly into account multiple scatterings only up to the third order. The duration of the calculations is proportional to the number of slice configurations taken into account. There are no limitations in respect of disorder or strength of scattering.

## 5. Conclusions

Compositional disorder has important implications for the electronic characteristics of quantum wires with small lateral dimensions. Using the preferred (subband) basis for this problem allow us to see explicitly the influence of disorder on the wire 1D subbands. Our results give strong indication that for achievement of good quality bulk quantum wire lasers it is necessary to avoid islands of strongly scattering materials within the wire and to reduce interface roughness of wires. The CPA calculations provide us with density of states characteristics that are useful for the estimations of

potential optical properties of quantum wire structures. The efficiency of using CPA is only limited by the number of relevant configurations of slices that we have in the system.

If there is correlation from slice to slice of the wire, then this effectively only smooths locally the wire and broadens it (for the case when $\lambda \leqslant l_c$, where $\lambda$ is longitudinal wavelength of electron and $l_c$ is the longitudinal correlation length of the wire). In this case the density of states diagram will be shifted towards lower energies and broadening will decrease in comparison with uncorrelated boundary roughness.

## Acknowledgments

We thank the SERC for supporting our computing facilities. KN also wishes to thank The Serbian Science Foundation and The British Scholarship Trust for Yugoslavs for financial support.

## References

[1] Sakaki H 1980 *Japan J. Appl. Phys.* **19** 94
[2] Arakawa Y and Sakaki H 1982 *Appl. Phys. Lett.* **40** 939
[3] Weisbuch C, Dingle R, Gossard A C and Wiegmann W 1980 *J. Vac. Sci. Technol.* **17** 1128
Miller R S, Tsang W and Munteanu O 1982 *Appl. Phys. Lett.* **41** 374
[4] Sakaki H 1984 *Proc. Int. Symp. Foundations of Quantum Mechanics (Tokyo, 1983)* ed S Kamefuchi *et al* (Tokyo: Physical Society of Japan) pp 94–110
[5] Neave J H, Dobson P J, Joyce B A and Zhang J 1985 *Appl. Phys. Lett.* **47** 100
Petrof P M, Gossard A C and Weigmann W 1984 *Appl. Phys. Lett.* **45** 620
[6] Soven P 1967 *Phys. Rev.* **156** 809
Taylor D W 1967 *Phys. Rev.* **156** 1017
[7] Hugill K J, Clarke S, Vvedensky D D and Joyce B A 1989 *J. Appl. Phys.* **66** 3415
[8] (a) Tsukada M 1969 *J. Phys. Soc. Japan* **26** 684
(b) Butler W H 1973 *Phys. Rev.* B **8** 4499
[9] Ducastelle F 1974 *J. Phys. C: Solid State Phys.* **7** 1795
[10] Elliot R J, Krumhansl J A and Leath P L 1974 *Rev. Mod. Phys.* **46** 465
[11] MacKinnon A 1985 *Z. Phys.* B **59** 385
[12] Kaplan T and Gray L J 1981 *Excitations in Disordered Systems* ed M F Thorpe (New York: Plenum) p 129–43
[13] Kirkpatrick S and Eggarter T P 1972 *Phys. Rev.* B **6** 3598
[14] Taylor J P, Hugill K J, Vvedensky D D and MacKinnon A 1991 *Phys. Rev. Lett.* **67** 2359
Taylor J P 1990 *PhD Thesis* Imperial College of Science, Technology and Medicine, London, UK
[15] Mašek J and B Kramer 1989 *Z. Phys.* B **75** 37
[16] Dean P and Martin J L 1960 *Proc. Roy. Soc.* A **259** 409
[17] Evangelou S N 1986 *J.Phys. C: Solid State Phys.* **19** 4291